Fretting about FRET: Correlation between κ and R

Darren B. VanBeek, Matthew C. Zwier, Justin M. Shorb, and Brent P. Krueger
Hope College, Department of Chemistry, Holland, Michigan

ABSTRACT Molecular dynamics simulations were used to examine the structural dynamics of two fluorescent probes attached to a typical protein, hen egg-white lysozyme (HEWL). The donor probe (D) was attached via a succinimide group, consistent with the commonly-used maleimide conjugation chemistry, and the acceptor probe (A) was bound into the protein as occurs naturally for HEWL and the dye Eosin Y. The $\langle\kappa^2\rangle$ is found to deviate significantly from the theoretical value and high correlation between the orientation factor κ and the distance R is observed. The correlation is quantified using several possible fixed A orientations and correlation as high as 0.80 is found between κ and R and as high as 0.68 between κ^2 and R. The presence of this correlation highlights the fact that essentially all fluorescence-detected resonance energy transfer studies have assumed that κ and R are independent—an assumption that is clearly not justified in the system studied here. The correlation results in the quantities $\langle\kappa^2 R^{-6}\rangle$ and $\langle\kappa^2\rangle\langle R^{-6}\rangle$ differing by a factor of 1.6. The observed correlation between κ and R is caused by the succinimide linkage between the D and HEWL, which is found to be relatively inflexible.

INTRODUCTION

Fluorescence-detected resonance energy transfer (FRET) has been an important tool in structural biology for more than three decades (1–19). Recently, with the availability of single-molecule microscopes and a wide array of techniques for fluorescently labeling proteins and nucleic acids both in vitro and in vivo, the number of studies that utilize FRET has expanded dramatically (Google scholar, in 2005, yielded more than 2000 references that included ''FRET''). While FRET is now being applied to a tremendous variety of systems utilizing an array of experimental techniques, many of which could only be imagined while FRET was maturing, most modern FRET studies still make use of the same 30+-year-old approximations, often with little consideration of their applicability to the particular system of study. Here, we present computational examination of the correlation between orientation and distance (κ and R_{DA}, respectively, see below) between the two fluorescent probes. The independence of these two factors has been assumed in the vast majority of FRET studies, yet, to the author's knowledge, has been examined in only two articles (20,21) and even mentioned in only four others (1,22–24). This independence approximation clearly breaks down in the chosen system and the physical cause of the breakdown appears to be a quite general result of the commonly-used succinimide linkage between fluorescent label and protein.

In FRET studies, a fluorescence observable is used to determine the rate of resonant energy transfer (k_{RET}) from an energy donor (D) to an energy acceptor (A), where D and A are typically fluorescent moieties that may be native to the system, added chemically, added genetically, or through some combination. The RET rate is often measured through time-resolved experiments that give k_{RET} more-or-less directly or through steady-state experiments that give k_{RET} indirectly via the efficiency of D to A energy transfer relative to D fluorescence. This rate can be related to the distance between the D and A, R_{DA}, through theory developed by Förster in the 1940s (25–27). The Förster equation appears in many forms (1,2,25,28) such as

$$k_{RET} = \frac{9(\ln 10)\kappa^2\phi_D}{128\pi^5 N_A n^4 R_{DA}^6 \tau_D}\int_0^\infty N f_D(\tilde{\nu})\epsilon_A(\tilde{\nu})\tilde{\nu}^{-4}\,d\tilde{\nu}, \quad (1)$$

where ϕ_D is the fluorescence quantum yield of the D, τ_D is the excited state lifetime of the D in the absence of RET, n is the refractive index of the medium, and κ describes the relative orientation of the D and A and is defined below. The integral is called the spectral overlap, J_{DA}, and contains the normalized emission spectrum of the D, $N f_D(\tilde{\nu})$, and the absorption spectrum of the A, $\epsilon_A(\tilde{\nu})$, on a wavenumber scale. Note that the values of ϕ_D, τ_D, and J_{DA} have been tabulated for many D-A pairs (28) and are generally taken to be independent of any structural dynamics in the system such that

$$k_{RET} = C\kappa^2 R_{DA}^{-6}. \quad (2)$$

If one assumes a particular value for κ^2 (often 2/3, see below) then the measured k_{RET} can be related to the valuable structural parameter, R_{DA}. Since the locations of the D and A on the system of interest are usually well-known, one has now learned something about the structure of the protein or nucleic acid under investigation. Or, if the D and A are attached to two different bodies, one has an easily-observed assay of whether those two bodies are bound or not, allowing determination of, e.g., the ΔG of binding.

In the 1970s and 80s, pioneering researchers convincingly showed the broad applicability of a number of approximations that proved useful in analysis of FRET data (3–5,29–33).

Submitted July 3, 2006, and accepted for publication January 8, 2007.

Address reprint requests to B. P. Krueger, Tel.: 616-395-7629; E-mail: kruegerb@hope.edu.

0006-3495/07/06/4168/11 $2.00

doi: 10.1529/biophysj.106.092650

Most famous of these is the ''κ^2 approximation'' mentioned above. The value κ is defined as

$$\kappa = \hat{\mu}_D \cdot \hat{\mu}_A - 3(\hat{\mu}_D \cdot \hat{R}_{DA})(\hat{\mu}_A \cdot \hat{R}_{DA}), \quad (3)$$

where $\hat{\mu}_D$ and $\hat{\mu}_A$ are unit vectors along the transition dipoles of the D and A, respectively, and $\hat{R}_{DA}$ is the unit vector along the line connecting the centers of the D and A. If the D and A are free to independently sample all possible orientations, the average value of κ^2 can be determined analytically to be 2/3. The validity of this isotropic limit was the focus of many early FRET articles and a number of methods were developed to reduce the uncertainty in R_{DA} resulting from uncertainties in $\langle\kappa^2\rangle$ (5,31,32,34–39). More recently, associated anisotropy measurements have been used to verify whether a distribution in FRET efficiencies results from a distribution of distances or a distribution in orientational mobility of the D (19,40). Despite these efforts, most experiments to date have simply assumed the value of 2/3 and their general success suggests that under many common conditions the difference between the actual $\langle\kappa^2\rangle$ and 2/3 leads to modest errors in determining R_{DA} (18,28,37,41).

However, by substituting the average value of κ^2 into Eq. 2, every researcher that has thoughtfully (or blindly) employed the κ^2 approximation has implicitly also assumed that κ^2 is independent of R_{DA}, i.e., that

$$\langle\kappa^2 R_{DA}^{-6}\rangle = \langle\kappa^2\rangle \langle R_{DA}^{-6}\rangle. \quad (4)$$

Indeed, not one of the methods mentioned above that strive to account for various degrees of probe motion in $\langle\kappa^2\rangle$ has given any notice to the effects of correlation between κ and R_{DA} (5,31,32,34–39). This approximation—the independence of κ and R_{DA}—has been examined only briefly and not at all in the past two decades to the authors' knowledge. In a series of articles published in the 1970s, Dale and co-workers extensively discussed the interplay of κ and R_{DA} on k_{RET}. These articles included discussion of κ^2 being averaged in either the dynamic or static limits. These authors did mention the possibility of correlation between κ and R_{DA} and that this would make retrieval of R_{DA} from a measurement of k_{RET} difficult, but no detailed examination was performed (22). Also in the 1970s, Englert and co-workers conducted a number of remarkable (for their time) molecular mechanics studies of the motions of probe molecules on peptides and did find some evidence of correlation between κ and R_{DA}, though the force field and methods employed in these works were necessarily crude by today's standards (20,21).

More recently, a number of groups have used molecular dynamics (MD) simulations to aid understanding of FRET experiments (23,24,42–48). Many of these works (23,24,42,46–48) examined $\langle\kappa^2\rangle$ and found varying degrees of agreement between their simulations and the isotropic limit. Four of these works (23,24,42,47) carefully evaluated the electronic coupling between donor and acceptor at every snapshot and, therefore, did properly account for correlation between κ and R_{DA}, though only two actually mentioned the possibility (23,24) and neither treated it in detail.

While the success of many careful FRET experiments suggests that κ and R_{DA} must be reasonably independent in most cases, it is important to note that for most of its history of use in biology, FRET has been applied to proteins that are small, rigid, and soluble. In contemporary studies, FRET is being applied to systems of remarkable diversity including soluble proteins, membrane proteins, and nucleic acids of almost every conceivable shape and size as well as large protein-protein and protein-nucleic acid complexes. Many of these systems are also far from rigid, undergoing large-scale structural changes. Since κ and R_{DA} are both structural parameters describing similar molecules in similar environments, it is reasonable to expect that there is a variety of systems in which D-A relative orientation and D-A distance show some degree of correlation. Thus, it is prudent to examine the effect such correlation might have on FRET results in a variety of systems. We begin to explore this arena here, presenting the results of one such examination using the archetypal protein, hen egg-white lysozyme (HEWL).

In the system we have chosen to study (shown in Fig. 1), the D (7-dimethylamino-4-methylcoumarin, i.e., DACM) is attached to HEWL via a succinimide linkage as in typical maleimide conjugation chemistry. The A (Eosin Y, i.e., eosin) binds noncovalently, meaning that its orientation is essentially fixed relative to the protein (49–53). While this is an unusual arrangement compared to classic FRET studies in which both D and A are on flexible linkages, common use of intrinsic probes (e.g., NADP) and the growing popularity of the FlAsH family of fluorescent labels (54) as well as GFP and related fluorophores makes this a system of broad practical interest for contemporary FRET studies, in addition to providing a useful test of the independence of κ and R_{DA}.

The computational methods employed here are described below followed by detailed analysis of the behavior of κ and R_{DA}. Significant correlation between κ and R_{DA} is observed as well as significant deviation of $\langle\kappa^2\rangle$ from the theoretically predicted value. The physical basis for the failure of the κ^2 approximation and the independence approximation is discussed as well as the impact of these results on FRET experiments.

MATERIALS AND METHODS

Because the fluorescent labels represent residues not present in the standard AMBER force fields, their parameterization was required. Atom types for both molecules were chosen through analogy to the generalized AMBER force field (GAFF) (55), which is designed to be compatible with the Cornell et al. force field (56). Normal mode calculations performed using the nmode package of the AMBER 8 suite (57) (University of California, San Francisco, CA) revealed generally good agreement with vibrational modes calculated quantum mechanically (QM) at the DFT(B3-LYP)/6-31G* level and scaled by 0.96 (58). All QM calculations were performed using the 1998 version of the Gaussian suite (59) (Gaussian, Pittsburgh, PA). However, the molecular mechanics description of the out-of-plane bending motions of the heterocyclic

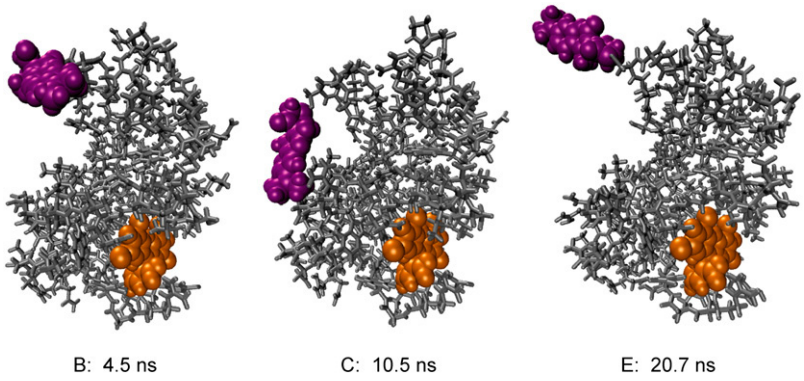

FIGURE 1 Structures of the simulation system from three different snapshots. Each is labeled according to the probe orientation family it represents and its time. The HEWL protein is shown with gray bonds. The DACM donor and eosin acceptor dyes are shown with purple and orange Van der Waals spheres, respectively. In the family C structure, DACM interacts closely with Val-109, Arg-112, and Asn-113. Images generated using VMD (84).

oxygen present in both molecules were found to be highly exaggerated relative to the QM calculations—amplitudes too high and frequencies too low. Reviewing the parameters revealed that the x-CA-OS-x dihedral parameter in GAFF (not present in Cornell et al.) had a force constant ($V_n/2$) of 1.8 kcal/mol, similar to that between tetrahedral carbons. However, in both dye molecules the involved atoms are part of the aromatic ring system such that we might expect a force constant similar to that found for a six-membered ring of aromatic carbon atoms, or 14.5 kcal/mol for both GAFF and Cornell et al. Adjusting the force constant and repeating the normal mode calculations revealed the best agreement with scaled QM frequencies for a force constant of ≈18 kcal/mol, similar to the aromatic carbon force constant. A new atom type was defined—aromatic oxygen, OA—to represent the heterocyclic oxygen present in the aromatic ring systems of many fluorescent probes. For generality and consistency with the force field of Cornell et al., the x-CA-OA-x force constant was assigned a value of 14.5 kcal/mol. All other force constants were assumed to be the same as the OS atom type in GAFF. Charges for both molecules were determined using the RESP package of AMBER 8, which involves restrained fitting to an electrostatic potential derived quantum-mechanically at the HF/6-31G* level (60,61). Structures, assigned atom types, and partial charges for DACM and eosin are provided as Supplementary Material.

The starting structure of HEWL was taken from the microgravity crystal structure (PDB ID: 1BWH) (62) with all waters removed. Residue 47 was changed from threonine to cysteine and bonded to the dye DACM (63,64) via a succinimide group as shown in Fig. 2. This structure was minimized to remove bad Van der Waals contacts. Eosin was placed near the binding site using the xLeap package within the AMBER suite and restraints were

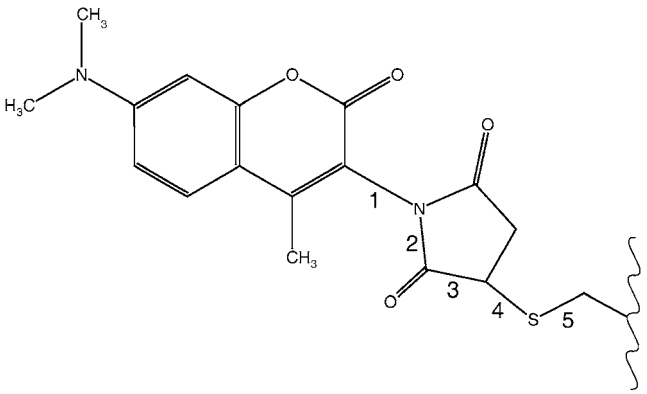

FIGURE 2 Chemical structures showing the DACM dye, succinimide linkage, and cysteine side chain. The five dihedral angles discussed in the text are indicated with numbers near the central bond. Rotational freedom of these dihedral angles are shown in Fig. 8.

invoked to pull the eosin into the binding site during a short MD run. The restraints were chosen to encourage the eosin to bind as deduced from multiple spectroscopic studies and shown in Jordanides et al. (49). The system was then neutralized by adding 5 Cl^- ions and solvated with a 20 Å buffer of explicit water for a total of 17,712 water molecules (total system size 55,149 atoms). The restraints were removed and all further MD was performed without any restraints.

All MD simulations were performed with the Sander package of AMBER 8 using the isothermal-isobaric (*NPT*) ensemble. A cutoff of 9 Å was used for Van der Waals interactions and particle mesh Ewald (65,66) was used for electrostatic interactions. SHAKE was applied to all bonds with hydrogen (67). The system was equilibrated in four steps:

1. During 5 ps of MD with 1 fs steps and tight temperature and pressure couplings, the target temperature was raised from 0 to 60 K.
2. With 2 fs steps, 20 ps of MD were used to raise the target temperature to 298 K.
3. Over 25 ps (2 fs steps) the temperature and pressure coupling were gradually relaxed to values of 10 ps for each.
4. A final 100 ps equilibration was conducted with conditions identical to production MD (2 fs steps, 298 K, temperature and pressure coupling constants of 10 ps).

System equilibration was confirmed by noting that drifts in the total energy and density (as measured by the slopes of linear fits to the final 25 ps of equilibration data) were $< 5\%$ of the short-term fluctuations in each (as measured by the standard deviation). The diffusion of the chloride ions was also measured; all five continued to diffuse with similar diffusion constants through the simulation, confirming that none of the counterions interacted for long times with any specific protein sites.

A total of 37 ns of production MD was generated and system coordinates were saved every 200 fs, yielding 185,000 snapshots constituting roughly 700 GB of total structural data. From each coordinate snapshot, the positions and orientations of the two dye molecules were retrieved. The centers of the fluorophores were defined by the mass-weighted average positions of the atoms determined to be involved in the transition. Atoms were judged to be involved in the transition by visual inspection of the transition densities determined at the CIS/6-31G* level. The CIS calculation also provides the orientation of the transition dipole for each dye. A pair of atoms was chosen such that the orientation of the vector between them most closely matched the orientation of the calculated transition dipole. The vector connecting these atoms was then used as a measure of the transition dipole orientation throughout the simulation. The angles between the QM-determined transition dipoles and the atomic approximations to the transition dipoles are 1.75° and 0.002° for DACM and eosin, respectively.

Note that the definition of the transition dipole direction of each probe comes from a single QM calculation performed on an optimized structure of each dye without solvent. This kind of analysis makes two assumptions about the D and A transition dipoles: 1) that the transitions between ground and excited states in both the D and A are each well described by a single

transition dipole, fixed to the molecular framework; and 2) that that transition dipole for each probe is insensitive to fluctuations in its environment.

Regarding the first assumption, the Steinberg group pointed out that for a number of common fluorescent probes, the transitions between ground and excited states are better described as a mixture between multiple transitions and, therefore, should be described using multiple transition moments (68). This mixing is particularly important for naphthalene, the subject of the original Steinberg work, as well as the ubiquitous fluorescence probe tryptophan. As an example, the complex fluorescence behavior of tryptophan arises because two low-lying excited singlet states, ^1L_a and ^1L_b, are nearly degenerate and nearly orthogonal in their transition dipole orientations. Thus, at many excitation wavelengths, a mixture of the two states is generated, leading to complex photophysical behavior that is revealed through polarization spectroscopy (69–72). In contrast, the DACM and eosin used in this study exhibit simple excited-state behavior. Their fluorescence anisotropies are not significantly wavelength-dependent (data not shown) (73); their time-resolved anisotropies decay from an initial value near the theoretical limit of 0.4 (52,73); and the S_1 state responsible for absorption and emission is energetically well separated from other states (based on our CIS calculations and absorption/emission spectra). Thus, the assumption of a single, fixed transition dipole is well-justified for both DACM and eosin. In fact, many commonly employed probe molecules (e.g., coumarins, xanthenes, and AlexaFluor dyes) exhibit this ideal behavior (74–76) such that the analysis methods utilized here are reasonable for a large number of FRET systems.

The second assumption can be addressed computationally by evaluating the electronic structure of each probe molecule at each dynamics snapshot (47,77,78). This treatment allows fluctuations in both the transition dipole orientation and magnitude to be accounted for. However, this QM evaluation of every snapshot is computationally intensive, particularly for a trajectory of ~40 ns, and is beyond the scope of the present work.

While accurately representing the molecular transition moments of the D and A is important for modeling the RET behavior of this particular system, the general question of interest here centers on the relative motions of one free and one fixed probe in any system with any arbitrary preferred D-A orientation. Therefore, to more generally report on the consequences of having one free and one fixed probe, we should consider the possibility that the A might bind in any orientation relative to the protein. To address this broader question, we also kept track of an alternate transition dipole for eosin, roughly perpendicular to the actual transition dipole and still in the plane of the aromatic core of the molecule. This transition dipole will be referred to using a y subscript (e.g., the κ factor between this transition dipole and the DACM transition dipole is κ_y). Taking the cross product of these two vectors provides a second alternate transition dipole (z), such that the group of three approximately form a three-dimensional basis for appraising the general ramifications to FRET of having one fixed and one free probe.

RESULTS AND DISCUSSION

Structural dynamics

The primary data retrieved from each snapshot of the MD simulation were the orientation of the DACM and eosin transition dipoles and the vector connecting the centers of the dyes, which will be discussed extensively below. However, we will first assess the integrity of the eosin-HEWL complex—an important test since no specific restraints were used to hold the eosin into the protein and because the eosin-HEWL complex is characterized by a modest K_d of 23 μM (A. J. Huisman, L. R. Hartsell, B. P. Krueger, and M. J. Pikaart, unpublished). The distance between five different eosin atoms and nearby side chains in the protein were measured at each snapshot. These distances showed small fluctuations about their average values and never showed any large values that would be indicative of unbound eosin (data not shown). Thus, we can be confident that the eosin was bound to the HEWL throughout the full simulation.

Over the course of the ≈40 ns of MD simulation, the system samples from a variety of structural families. With respect to the motions of the protein, a two-dimensional RMSD plot is useful for identifying the relationships between these different families. The all-atom (not including the fluorescent probes) two-dimensional RMSD plot (Fig. 3) shows the pairwise difference in structure of each snapshot to every other snapshot. (Due to limited resolution of the figure, snapshots every 200 ps were used.) These data indicate that the protein is free to fluctuate between a number of different structures and that the final structures are not dramatically different from the early structures. In turn, these suggest that the system is reasonably well equilibrated at the outset and that the protein is not artificially inhibited by some artifact of the simulation, but is free to sample conformational space. Significant structural transitions are observed at 5.6 ns, 10.2 ns, 15.2 ns, 28.7 ns, and 30.3 ns. A number of minor transitions between 15.2 and 28.7 ns and between 30.3 ns and the end could be identified as well, but as this work focuses on the behavior of the fluorescent probes, the detailed structural dynamics of the protein will not be discussed.

To identify whether the structural transitions identified through Fig. 3 are manifested in the behavior of the fluorescent probes, the trajectories of the D-A distance, R_{DA}, and the three κ factors (κ, κ_y, κ_z) were examined (Fig. 4). These

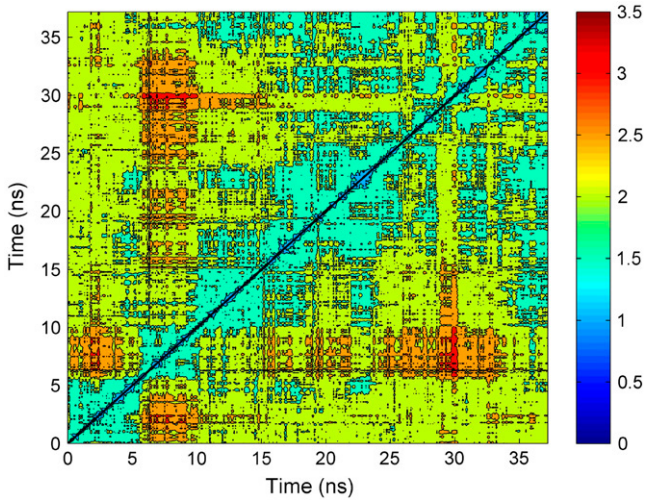

FIGURE 3 Two-dimensional RMSD plot for the HEWL protein (dyes were not included). Snapshots were taken every 200 ps and the RMSD was measured using all atoms. The vertical scale units are Å. Low RMSD values off-diagonal indicate structures that are similar to each other. Squares of low RMSD along the diagonal (e.g., 0–6 ns) indicate time periods when the protein structure fluctuated about some average position, but remained roughly the same. Junctions between these squares (e.g., ≈6 ns) indicate transitions from one structural family to another.

data were used, independent of Fig. 3, to identify transition times and different probe orientation families. Our goal was not to perfectly separate different statistical regions of κ and R_{DA} behavior, but to roughly group similar regions to yield a modest number of families with identifiable characteristics. Transitions between families were determined based on visual inspection of the κ and R_{DA} trajectories, using obvious shifts in the value of either parameter (e.g., at 8.22 ns and 11.79 ns) or spikes in either parameter accompanied by changes in the fluctuations of either parameter (e.g., 4.35 ns and 25.77 ns). Thus, the simulation was, rather arbitrarily, divided into eight time regions, which will be identified as probe orientation families *A–H*. The transition times and statistical characteristics of each family are given in Tables 1 and 2, and plots of the distributions of κ and R_{DA} for some families are shown in Fig. 5. (Distributions for all families are given in Supplementary Material Figs. S3 and S4.) It is clear from Tables 1 and 2 and Fig. 5 that there are a number of distinct families of κ and R_{DA} behavior and that these distinctions are paralleled in the two quantities. For instance, the families with the three highest mean κ values, *E*, *F*, and *G*, exhibit three of the four highest R_{DA} values. Family *D* shows the highest κ standard deviation as well as the highest R_{DA} standard deviation, in contrast to family *C*, which shows the lowest standard deviations in both κ and R_{DA}. Thus, it is clear that, at the family-to-family timescale, there is some degree of correlation between κ and R_{DA}. This will be explored further after discussion of various calculations of RET rates.

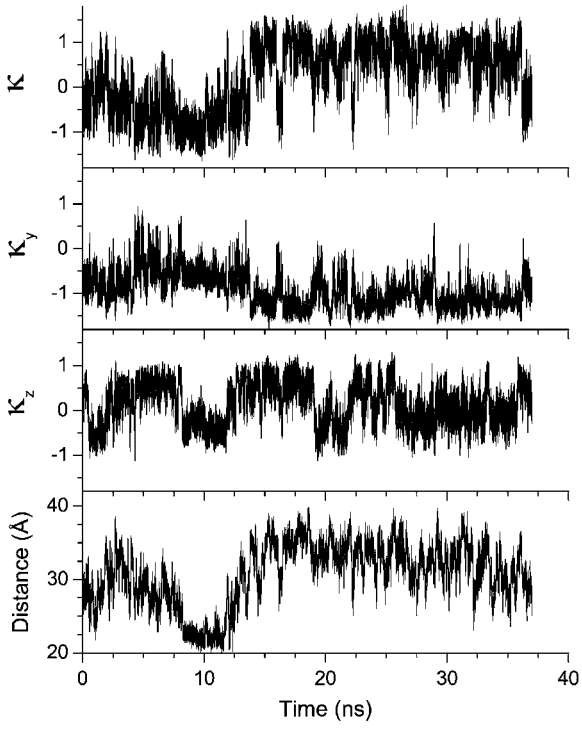

FIGURE 4 Trajectories of the distance between the D and A and of the κ factors for the three different A representations. Transitions between different probe orientation families were identified from these data. Transition times are given in Table 1.

Resonant energy transfer

The electronic interactions that promote RET between the eosin and DACM can be evaluated by examining just the two structural parameters, κ and R_{DA}. Provided the ideal dipole approximation (IDA) holds, use of the simple expression given in Eq. 2 is justified. Given that the two dyes are reasonably far apart in this system (>20 Å), we expect the IDA to be valid. In cases where the IDA is suspect, several groups have developed methods for accurately evaluating the D-A interactions (80–83). While these methods are computationally more demanding than simply evaluating Eq. 2, their implementation is straightforward and practical application in conjunction with MD simulations has been demonstrated (23,42). For systems in which one dye is fixed and the other is free, in principle, to sample all space, $\langle\kappa^2\rangle$ depends on the angle between the fixed transition dipole (A in this case) and the vector connecting the centers of the probes such that (5,28)

$$\langle\kappa_T^2\rangle = \frac{1}{3} + (\hat{\mu}_A \cdot \hat{R}_{DA})^2. \quad (5)$$

For the three A transitions considered here, the mean angles between $\hat{\mu}_A$ and $\hat{R}_{DA}$ (taken from the MD simulations) are ~39°, 124°, and 75°, which give theoretical $\langle\kappa_T^2\rangle$ values of 0.93, 0.64, and 0.40, respectively, for the actual eosin transition, *y*, and *z*. The average values from the simulation are found to be $\langle\kappa^2\rangle = 0.621$, $\langle\kappa_y^2\rangle = 1.02$, and $\langle\kappa_z^2\rangle = 0.24$. The discrepancies between theoretical and observed values for all three of the $\langle\kappa^2\rangle$ suggest that the DACM motion is significantly restricted. Examination of the distribution of DACM transition dipole orientations after removing protein motion (Supplementary Material Fig. S5) suggests that it explores a fairly limited range of space. However, this visual inspection can be deceiving since the DACM need explore only one hemisphere of space to yield a $\langle\kappa^2\rangle$ that agrees with $\langle\kappa_T^2\rangle$. More quantitative analysis shows that 90.1% of the observed DACM orientations lie within 1.46π steradians or 36.6% of all possible orientations. For comparison, the tightly bound eosin has 99.6% of its distribution concentrated within 0.0744π steradians or 1.86% of all possible orientations (also shown in Supplementary Material Fig. S5). Thus, while the DACM is quite free to move relative to eosin, it does clearly explore a restricted portion of orientation space, supporting the observed deviation between $\langle\kappa_T^2\rangle$ and $\langle\kappa^2\rangle$.

It follows that replacing κ^2 with its theoretical average in Eq. 2 will lead to a poor estimate of the rate. Indeed, combining the theoretical $\langle\kappa_T^2\rangle$ value with the appropriate average distance factor, $\langle R_{DA}^{-6}\rangle = 2.00 \times 10^{-9}\text{Å}^{-6}$, yields average RET rates of $\langle k_{RET}^T\rangle = 1.86 \times 10^{-9}C$, $\langle k_{RETy}^T\rangle = 1.28 \times 10^{-9}C$, and $\langle k_{RETz}^T\rangle = 0.81 \times 10^{-9}C$, whereas using the $\langle\kappa^2\rangle$ value from the MD trajectory in Eq. 2, and assuming Eq. 4 is valid,

TABLE 1 Summary of the eight families of probe orientation behavior

			R_{DA}		κ			κ^2		
Family	Time range (ns)	Unc	Mean (Å)	SD (Å)	Mean	SD	Corr	Mean	SD	Corr
A	0–4.35	0.01	29.8	3.0	−0.26	0.48	0.42	0.30	0.37	−0.20
B	4.35–8.22	0.01	27.9	2.0	−0.63	0.43	0.64	0.58	0.50	−0.57
C	8.22–11.79	0.014	22.3	0.91	−0.80	0.33	0.22	0.76	0.49	−0.17
D	11.79–19.03	0.01	32.5	3.9	0.44	0.73	0.80	0.73	0.53	0.32
E	19.03–22.14	0.01	33.9	1.8	0.61	0.39	0.70	0.52	0.42	0.69
F	22.14–25.77	0.01	33.3	2.4	0.77	0.52	0.65	0.87	0.59	0.57
G	25.77–36.17	0.01	32.0	2.8	0.69	0.39	0.72	0.63	0.51	0.67
H	36.17–37	0.03	29.3	1.5	−0.34	0.34	0.25	0.23	0.24	−0.16
All	0–37	0.004	30.7	4.2	0.23	0.76	0.80	0.62	0.52	0.20

Corr is Pearson's linear correlation coefficient (R) between R_{DA} and the specified quantity. *Unc* is the maximum uncertainty in the correlation coefficient based on the value of the correlation and the population size.

yields the independently averaged rate, $\langle k_{RET}^{I} \rangle = 1.24 \times 10^{-9} C$, or $2.03 \times 10^{-9}\ C$ and $0.48 \times 10^{-9}\ C$ for y and z, respectively. Note that C is the set of constants that describe the spectral properties of DACM and eosin and is implied to contain the units of the rate (see Eqs. 1 and 2). (Because approximations relevant to these constants are not addressed here, all rates will be evaluated simply in terms of the dynamic structural parameters κ and R_{DA} and left in terms of C.) If, however, we do not assume Eq. 4 is valid—that is, we do not assume that κ and R_{DA} are independent—but instead evaluate Eq. 2 at each snapshot and then determine the average rate, we arrive at $\langle k_{RET} \rangle = 1.28 \times 10^{-9} C$, $\langle k_{RETy} \rangle = 1.27 \times 10^{-9} C$, and $\langle k_{RETz} \rangle = 0.43 \times 10^{-9} C$. Note that for the y transition dipole, the properly averaged rate is a factor of 1.6 smaller than when κ and R_{DA} are assumed to be independent and that for the z transition dipole, k_{RETz} is a factor of 1.9 smaller than assuming the theoretical average value for κ^2. These results are summarized in Table 3.

κ and R_{DA} correlation

The fact that $\langle \kappa^2 \rangle \langle R_{DA}^{-6} \rangle$ and $\langle \kappa^2 R_{DA}^{-6} \rangle$ yield such different values in the y case suggests that there is significant correlation between κ and R_{DA}. Fig. 6 shows a scatter plot of R_{DA} versus κ, which confirms that the two variables do depend on each other. The high extent of correlation between κ and R_{DA} is clearly shown in Fig. 7, an overlay of the κ and R_{DA} trajectories. Using linear regression of R_{DA} versus κ to quantify this correlation yields a correlation coefficient of 0.80 ± 0.001 for the eosin transition, -0.64 ± 0.002 for the y variant, and 0.34 ± 0.004 for z—all clearly nonzero. Of course, it is the correlation between κ^2 and R_{DA} that is important to RET. These correlation coefficients are 0.20 ± 0.004, 0.68 ± 0.002, and 0.07 ± 0.004 for the actual, y, and z transition dipoles, respectively.

The contrast in $\kappa - R$ and $\kappa^2 - R$ behavior for the three eosin transitions (actual, y, and z) is interesting. For the actual eosin transition, there is a high correlation between κ and R_{DA} and a much smaller (though still significant) correlation between κ^2 and R_{DA}. Despite the correlation coefficient of 0.20, the $\langle \kappa^2 \rangle \langle R_{DA}^{-6} \rangle$ and $\langle \kappa^2 R_{DA}^{-6} \rangle$ measures of k_{RET} differ by $<3\%$. Examination of Table 1 reveals that half of the eight families (the ones with $\langle \kappa \rangle > 0$) exhibit positive correlation between κ^2 and R_{DA}, and half negative correlation. Thus, good agreement between k_{RET}^{I} and k_{RET} is due to fortuitous cancellation of error over multi-nanosecond timescales (comparable to the D excited-state lifetime) because the value of κ fluctuates roughly equally about zero. For the y variant, the correlation between $\langle \kappa_y^2 \rangle$ and R_{DA} is higher than that between κ_y and R_{DA} (Table 2). In this case, the particular

TABLE 2 Summary of the eight families of probe orientation behavior for the alternate (*y* and *z*) acceptor transition dipoles

		κ_y			κ_y^2			κ_z			κ_z^2		
Family	Unc	Mean	SD	Corr	Mean	SD	Corr	Mean	SD	Corr	Mean	SD	Corr
A	0.01	−0.80	0.30	−0.57	0.74	0.45	0.59	−0.01	0.48	0.58	0.23	0.20	−0.24
B	0.01	−0.40	0.38	−0.56	0.30	0.30	0.59	0.56	0.26	0.11	0.38	0.26	0.09
C	0.014	−0.62	0.17	−0.06	0.41	0.20	0.07	−0.36	0.22	−0.27	0.18	0.15	0.23
D	0.01	−1.06	0.37	−0.76	1.26	0.68	0.77	0.49	0.32	0.42	0.35	0.28	0.27
E	0.01	−0.99	0.36	−0.66	1.11	0.70	0.70	−0.31	0.35	0.60	0.22	0.22	−0.53
F	0.012	−1.18	0.23	−0.41	1.44	0.50	0.40	0.41	0.38	0.44	0.31	0.28	0.36
G	0.01	−1.11	0.25	−0.29	1.29	0.49	0.34	−0.05	0.34	0.44	0.12	0.17	0.02
H	0.03	−0.78	0.25	−0.13	0.67	0.36	0.15	0.41	0.28	0.24	0.25	0.22	0.19
All	0.004	−0.93	0.39	−0.64	1.02	0.64	0.68	0.13	0.47	0.34	0.24	0.24	0.07

Corr is Pearson's linear correlation coefficient (R) between R_{DA} and the specified quantity. *Unc* is the maximum uncertainty in the correlation coefficient based on the value of the correlation and the population size.

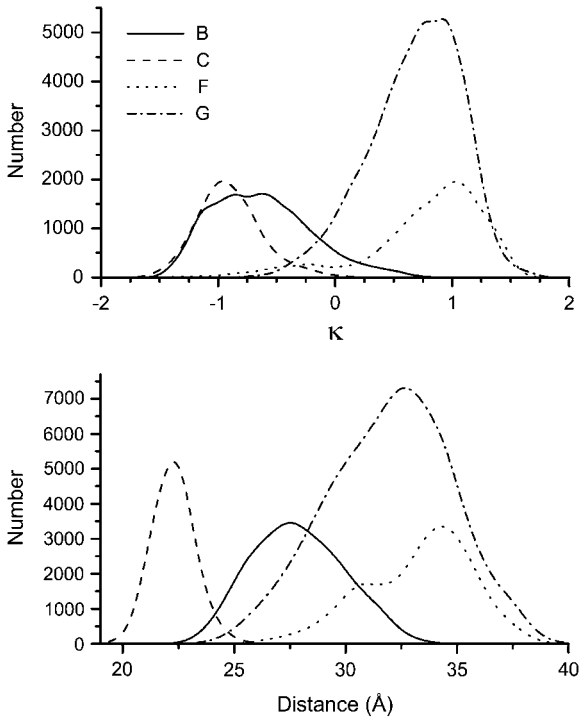

FIGURE 5 Histograms showing the distributions of κ (*upper panel*) and R_{DA} (*lower panel*) values for four of the eight probe orientation families. The distributions of all eight families are given in Supplementary Material Figs. S3 and S4. These four families illustrate the familial parallels in κ and R_{DA} behavior.

orientation of the A transition dipole is such that the $\langle\kappa_y^2\rangle$–R_{DA} correlation is always positive and mainly significant, larger than 0.3 for six of the eight families, leading to the large discrepancy between k_{RET} and k_{RET}^I. Finally, in the z variant, the correlation between $\langle\kappa_z^2\rangle$ and R_{DA} is generally small, <0.3 for six of the eight families leading to good overall agreement between k_{RET} and k_{RET}^I.

Tables 1 and 2 show that some of the probe orientation families exhibit high $\kappa - R_{DA}$ correlation (absolute value >0.3) for all three A transition dipoles (families *A*, *D*, *E*, and *F*) and some exhibit consistently low correlation (families *C* and *H*). Looking at family *C* more carefully reveals that its low correlation is the consequence of an instability in the relationship between κ and R_{DA}. Breaking family *C* into portions 1000-points (200 ps) long reveals correlation coefficients that range from -0.46 to 0.76. Thus, it is not that κ and R_{DA} are uncorrelated throughout family *C*; instead, there is a relationship between κ and R_{DA}, but that relationship is unstable and the positive and negative correlations cancel each other. (Because of its relatively small number of points, family *H* was not analyzed in this way.) Thus, if one looks at small enough timescales, timescales that are comparable to energy transfer times in many cases, the correlation between κ and R_{DA} is found to be significant at all points throughout the simulation. Note that the instability observed in family *C* is likely the result of DACM being bound to the surface of the protein (Fig. 1). This causes the fluctuations in both κ and R_{DA} to be small in magnitude such that their relationship can easily change from positively correlated to negatively correlated. Thus, ironically, the long-term correlation between κ and R_{DA} is smallest in this particular case when both probes are essentially fixed to the protein.

The fact that $\kappa - R_{DA}$ correlation in family *C* disappears as one averages over longer and longer timescales suggests that the overall correlation observed here might become less significant if the MD simulation were extended to μs or ms timescales. While this is certainly possible, it is important to note that the majority of probe orientation families found here exhibit significant $\kappa - R_{DA}$ correlation. Thus, for this system, correlation between κ and R_{DA} appears to be typical; lack of correlation is the exception. It follows that any new probe orientation families that might be sampled during a longer MD trajectory are likely to also exhibit $\kappa - R_{DA}$ correlation. As pointed out earlier and shown in Fig. 7, there is significant correlation over both short and long (family-to-family) timescales. The existence of multi-nanosecond correlation is supported by the fact that the overall $\kappa - R_{DA}$ correlation is larger than any of the individual family $\kappa - R_{DA}$ correlations. Thus, while we cannot guarantee that the 40 ns MD simulation has fully sampled representative dynamics of the D-lysozyme-A system, the observation of correlation between κ and R_{DA} (Fig. 7) throughout a variety of structural families (Fig. 3) suggests that extending the MD simulation to longer timescales may actually result in an increase in the observed overall $\kappa - R_{DA}$ correlation. Indeed, the $\kappa - R_{DA}$

TABLE 3 Summary of the different methods of computing the RET rate

Model	Rate ($\times 10^{-9}$ *C*)*			Assumptions
	Eosin	*y*	*z*	
$k_{RET}^T = \kappa_T^2 \langle R_{DA}^{-6}\rangle C$	1.86	1.28	0.81	$\kappa_T^2 = \frac{1}{3} + (\hat{\mu}_A \cdot \hat{R}_{DA})^2$; κ and R_{DA} independent; others†
$k_{RET}^I = \langle\kappa^2\rangle \langle R_{DA}^{-6}\rangle C$	1.24	2.03	0.48	κ and R_{DA} independent; others†
$k_{RET} = \langle\kappa^2 R_{DA}^{-6}\rangle C$	1.28	1.27	0.43	Others†

Model gives the expression used to compute k_{RET}. *Rate* gives the calculated value of k_{RET} for each of the three A transitions studied. *Assumptions* lists the assumptions that are appropriate for the given model.

**C* is the set of constants that describe the spectral properties of the D and A and is implied to contain the units of the rate; see Eqs. 1 and 2.

†*Others* means all other approximations required for Förster theory, such as the ideal dipole approximation and that *C* is constant with respect to structural fluctuations.

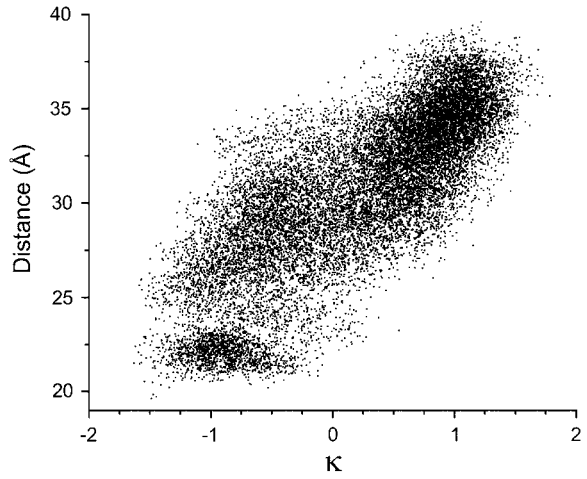

FIGURE 6 Scatter plot of R_{DA} against κ showing the correlation between them. Each dot represents a single snapshot; snapshots were taken every 2 ps of the simulation.

correlation coefficient for the first 20 ns of the simulation is 0.79, for the last 20 ns is 0.66, and overall is 0.80.

It is also important to note that there are two distributions with which the D and A sampling of space are important: the distribution of structures sampled over the same timescale as energy transfer, and the total distribution of structures. Even if the full set of relevant system structures do not exhibit correlation between κ and R_{DA}, it is clear that the $\kappa - R_{DA}$ correlation is significant over timescales relevant to energy transfer.

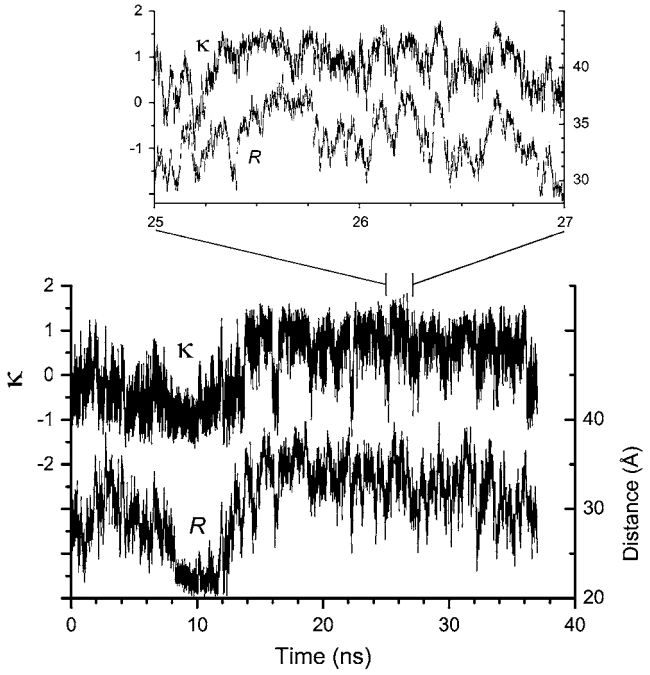

FIGURE 7 Trajectories of κ (*upper line*) and R_{DA} (*lower line*), showing the high degree of correlation between them. The main plot shows correlation over the full length of the trajectory while the inset highlights the short timescale correlation.

Physical basis of correlation

What is it that drives this correlation? It appears to be a result of the stiffness of the succinimide group that links the cysteine side chain with the DACM probe, and which results from the commonly-used maleimide conjugation chemistry. There is little flexibility in the connection between the coumarin skeleton of the dye and the five-membered ring of the succinimide, nor is the succinimide group itself very flexible. Thus, the motions of the dye are expected to be mainly due to flexibility about the β-carbon and sulfur of the cysteine side chain. Histograms of the motions of the five dihedral angles (defined in Fig. 2) are shown in Fig. 8. Dihedrals 1 and 2 each display a single peak, at 180° and 120°, respectively. Dihedral 4 displays more flexibility, but still samples a single peak for the majority of snapshots (180° ≈70% of the time). Dihedrals 3 and 5 show the most flexibility, with #3 sampling mainly two angles (60° and 180° totaling ≈90% of the snapshots) and #5 sampling strongly from three angles (≈50% at –60°, and ≈20% at 60° and 180°). The result of the relative inflexibility of the dye-protein linkage is that the dye behaves as though it is at the end of a long lever arm and, therefore, both its angular orientation with respect to the protein and its position are dependent on the conformation of the cysteine side chain.

It is likely that this correlation in angular orientation and spatial position with respect to the protein exists for most fluorescent molecules that are conjugated through maleimide chemistry. In the system of study here, the other dye (eosin) is essentially fixed relative to the protein so the correlation becomes apparent. In the more typical case where both

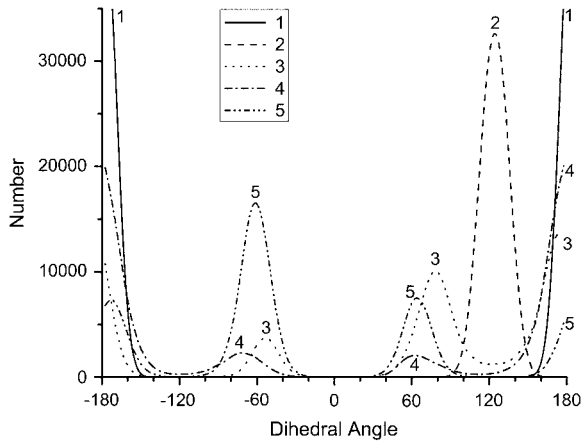

FIGURE 8 Histograms of the five dihedral angles that are critical to motion of the DACM probe. The identities of the angles are shown in Fig. 2. Dihedrals 1, 2, and 4 predominantly occupy just one orientation, while dihedral-3 mainly occupies two orientations. Only dihedral-5 samples significantly from three orientations.

probes are free to move, the relative motions of the two dyes are likely complex enough that the correlation becomes obscured in many cases.

While the results observed here are likely to be relevant to a wide variety of systems, the reader should bear in mind that the particular questions being addressed will determine their importance. As has been pointed out by many authors, the practical use of FRET as a structural probe is greatly aided by the R_{DA}^{-6} in Eq. 2. That large dependence of k_{RET} on R_{DA} translates to a small dependence of R_{DA} on k_{RET}. Thus, the 60% error in k_{RET_y} observed here when ignoring the correlation between κ_y and R_{DA} would translate into ~10% error in determining R_{DA} from an experimental value of k_{RET}. In many cases this amount error is significant, in many cases it is not. However, in all cases the validity of assuming that κ and R_{DA} are independent should be taken into consideration, along with the other FRET approximations. Finally, we note that the dynamic structural information determined here through MD simulations allows models for time-resolved emission decays of the D and A to be constructed (47). These models would allow direct comparison of the structural dynamics modeled by the simulation with experimentally measurable observables. Further analysis along these lines will be presented elsewhere.

CONCLUSION

MD simulations have been used to examine the structural fluctuations of an archetypal protein, HEWL, labeled in typical fashion with a donor dye, DACM, and noncovalently binding an acceptor dye, eosin, into a fixed pocket. Because of the structure of the linkage that results from the maleimide conjugation chemistry, the angular orientation and the spatial position of the DACM are related. This results in a significant degree of correlation between κ and R_{DA}, which yields a factor of 1.6 error in estimating k_{RET} when one assumes κ and R_{DA} are independent. The presence of correlation between κ and R_{DA} would lead to a noticeable (~10%) error in calculating R_{DA} from an experimental k_{RET} in this system. This correlation also highlights the fact that the standard treatment of FRET data assumes, among other things, the independence of κ and R_{DA}, though this has been rarely discussed in the literature. In addition, the $\langle\kappa^2\rangle$ value is quite different than the theoretical value for one free probe and one fixed probe. As the methods applied to study FRET, the systems studied with FRET, and the questions addressed by FRET all become broader and more complex, recognition of the κ and R_{DA} independence approximation, along with other FRET approximations, becomes increasingly more important.

SUPPLEMENTARY MATERIAL

An online supplement to this article can be found by visiting BJ Online at http://www.biophysj.org.

The authors thank Katie L. Hinkle for assistance with statistical analysis as well as Jacquelyn D. Lewis and Nora E. Kuiper for examination of the steady-state anisotropy behavior of DACM and eosin.

This work was generously supported by grants from Research Corporation, the American Chemical Society Petroleum Research Fund, the Howard Hughes Medical Institute, and the National Science Foundation Major Research Instrumentation and Research Experience for Undergraduates programs. Computer simulations were performed at the National Center for Supercomputing Applications. D.B.V. also recognizes the Beckman Foundation and Merck & Co. for their support.

REFERENCES

1. Clegg, R. M. 1996. Fluorescence resonance energy transfer. *In* Fluorescence Imaging and Microscopy. Chemical Analysis, Vol. 137. X. F. Wang, and B. Herman, editors. Wiley Interscience, New York.
2. Andrews, D. L., and A. A. Demidov. 1999. Resonance Energy Transfer. John Wiley & Sons, New York.
3. Stryer, L., and R. P. Haugland. 1967. Energy transfer: a spectroscopic ruler. *Proc. Natl. Acad. Sci. USA*. 58:719–726.
4. Stryer, L. 1978. Fluorescence energy transfer as a spectroscopic ruler. *Annu. Rev. Biochem.* 47:819–846.
5. Dale, R. E., and J. Eisinger. 1974. Intramolecular distances determined by energy transfer. Dependence on orientational freedom of donor and acceptor. *Biopolymers.* 13:1573–1605.
6. Pullerits, T., and A. Freiberg. 1991. Picosecond fluorescence of simple photosynthetic membranes: evidence of spectral inhomogeneity and directed energy transfer. *Chem. Phys.* 149:409–418.
7. Hochstrasser, R. A., S. M. Chen, and D. P. Millar. 1992. Distance distribution in a dye-linked oligonucleotide determined by time-resolved fluorescence energy transfer. *Biophys. Chem.* 45:133–141.
8. Akimoto, S., S. Takaichi, T. Ogata, Y. Nishimura, I. Yamazaki, and M. Mimuro. 1996. Excitation energy transfer in carotenoid-chlorophyll protein complexes probed by femtosecond fluorescence decays. *Chem. Phys. Lett.* 260:147–152.
9. Yang, M., and D. P. Millar. 1997. Fluorescence resonance energy transfer as a probe of DNA structure and function. *Methods Enzymol.* 278:417–444.
10. Jia, Y., D. S. Talaga, W. L. Lau, H. S. M. Lu, W. F. DeGrado, and R. M. Hochstrasser. 1999. Folding dynamics of single GCN-4 peptides by fluorescence resonant energy transfer confocal microscopy. *Chem. Phys.* 247:69–83.
11. Reddy, L. G., L. R. Jones, and D. D. Thomas. 1999. Depolymerization of phospholamban in the presence of calcium pump: a fluorescence energy transfer study. *Biochemistry.* 38:3954–3962.
12. Klostermeier, D., and D. P. Millar. 2002. Time-resolved fluorescence resonance energy transfer: a versatile tool for the analysis of nucleic acids. *Biopolymers.* 67:159–179.
13. Wang, D., and E. Geva. 2005. Protein structure and dynamics from single-molecule fluorescence resonance energy transfer. *J. Phys. Chem. B.* 109:1626–1634.
14. Bradforth, S. E., R. Jimenez, F. van Mourik, R. van Grondelle, and G. R. Fleming. 1995. Excitation transfer in the core light-harvesting complex (lh-1) of *Rhodobacter sphaeroides*: an ultrafast fluorescence depolarization and annihilation study. *J. Phys. Chem.* 99:16179–16191.
15. Zhuang, X., L. E. Bartley, H. P. Babcock, R. Russell, T. Ha, D. Herschlag, and S. Chu. 2000. A single-molecule study of RNA catalysis and folding. *Science.* 288:2048–2051.
16. Stryer, L. 1968. Fluorescence spectroscopy of proteins. *Science.* 162: 526–533.
17. Wallrabe, H., and A. Periasamy. 2005. Imaging protein molecules using FRET and FLIM microscopy. *Curr. Opin. Biotechnol.* 16:19–27.
18. Schuler, B., E. A. Lipman, P. J. Steinbach, M. Kumke, and W. A. Eaton. 2005. Polyproline and the ''spectroscopic ruler'' revisited

with single-molecule fluorescence. *Proc. Natl. Acad. Sci. USA*. 102: 2754–2759.

19. Johnson, C. K., B. D. Slaughter, J. R. Unruh, and E. S. Price. 2006. Fluorescence probes of protein dynamics and conformations in freely diffusing molecules: single-molecule resonance energy transfer and time-resolved fluorescence methods. *In* Reviews in Fluorescence, Vol. 3. C. D. Geddes and J. R. Lakowicz, editors. Springer, New York.
20. Englert, A., and M. Leclerc. 1978. Intramolecular energy transfer in molecules with a large number of conformations. *Proc. Natl. Acad. Sci. USA*. 75:1050–1051.
21. Leclerc, M., S. Prémilat, and A. Englert. 1978. Nonradiative energy transfer in oligopeptide chains generated by a Monte Carlo method including long-range interactions. *Biopolymers*. 17:2459–2473.
22. Dale, R. E., and J. Eisinger. 1976. Intramolecular energy transfer and molecular conformation. *Proc. Natl. Acad. Sci. USA*. 73:271–273.
23. Jean, J. M., and B. P. Krueger. 2006. Structural fluctuations and excitation transfer between adenine and 2-aminopurine in single-stranded deoxytrinucleotides. *J. Phys. Chem. B*. 110:2899–2909.
24. Srinivas, G., and B. Bagchi. 2001. Effect of orientational motion of mobile chromophores on the dynamics of Förster energy transfer in polymers. *J. Phys. Chem. B*. 105:9370–9374.
25. Förster, T. 1965. Delocalized excitation and excitation transfer. *In* Modern Quantum Chemistry, Vol. III. O. Sinanoglu, editor. Academic Press, New York.
26. Förster, T. 1946. Energy migration and fluorescence. *Naturwiss*. 33: 166–175.
27. Förster, T. 1948. Intermolecular energy transference and fluorescence. *Ann. Phys*. 2:55–75.
28. Van Der Meer, B. W., G. I. Coker, and S. Y. S. Chen. 1994. Resonance Energy Transfer: Theory and Data. VCH Publishers, New York.
29. Steinberg, I. Z., and E. Katchalski. 1968. Theoretical analysis of the role of diffusion in chemical reactions, fluorescence quenching, and nonradiative energy transfer. *J. Chem. Phys*. 48:2404–2410.
30. Haugland, R. P., J. Yguerabide, and L. Stryer. 1969. Dependence of the kinetics of singlet-singlet energy transfer on spectral overlap. *Proc. Natl. Acad. Sci. USA*. 63:23–30.
31. Dale, R. E., and J. Eisinger. 1975. Polarized excitation energy transfer. *In* Biochemical Fluorescence: Concepts, Vol. 1. R. F. Chen and H. Edelhoch, editors. Marcel Dekker, New York.
32. Dale, R. E. 1978. Fluorescence depolarization and orientation factors for excitation energy transfer between isolated donor and acceptor fluorophore pairs at fixed intermolecular separations. *Acta Phys*. A54:743–756.
33. Beardsley, K., and C. R. Cantor. 1970. Studies of transfer RNA tertiary structure by singlet-singlet energy transfer. *Proc. Natl. Acad. Sci. USA*. 65:39–46.
34. Eisinger, J., and R. E. Dale. 1974. Interpretation of intramolecular energy transfer experiments. *J. Mol. Biol*. 84:643–647.
35. Blumberg, W. E., R. E. Dale, J. Eisinger, and D. M. Zuckerman. 1974. Energy transfer in TRNAPHE (yeast). The solution structure of transfer RNA. *Biopolymers*. 13:1607–1620.
36. Dale, R. E., J. Eisinger, and W. E. Blumberg. 1979. The orientational freedom of molecular probes: the orientation factor in intramolecular energy transfer. *Biophys. J*. 26:161–194.
37. Haas, E., E. Katchalski-Katzir, and I. Z. Steinberg. 1978. Brownian motion of the ends of oligopeptide chains in solution as estimated by energy transfer between the chain ends. *Biopolymers*. 17:11–31.
38. Van Der Meer, B. W., M. A. Raymer, S. L. Wagoner, R. L. Hackney, J. M. Beechem, and E. Gratton. 1993. Designing matrix models for fluorescence energy transfer between moving donors and acceptors. *Biophys. J*. 64:1243–1263.
39. Wu, P., and L. Brand. 1992. Orientation factor in steady-state and time-resolved resonance energy transfer measurements. *Biochemistry*. 31: 7939–7947.
40. Rothwell, P. J., S. Berger, O. Kensch, S. Felekyan, M. Antonik, B. M. Wohrl, R. Restle, R. S. Goody, and C. A. M. Seidel. 2003. Multiparameter single-molecule fluorescence spectroscopy reveals heterogeneity of HIV-1 reverse transcriptase: primer/template complexes. *Proc. Natl. Acad. Sci. USA*. 100:1655–1660.
41. Amir, D., D. P. Levy, Y. Levin, and E. Haas. 1986. Selective fluorescent labeling of amino groups of bovine pancreatic trypsin inhibitor by reductive alkylation. *Biopolymers*. 25:1645–1658.
42. Ortiz, W., B. P. Krueger, V. D. Kleiman, J. L. Krause, and A. E. Roitberg. 2005. Energy transfer in the nanostar: the role of Coulombic coupling and dynamics. *J. Phys. Chem. B*. 109:11512–11519.
43. Srinivas, G., and B. Bagchi. 2000. Distribution of reaction times in diffusion controlled reactions in polymers. *Chem. Phys. Lett*. 328:420–424.
44. Srinivas, G., A. Yethiraj, and B. Bagchi. 2001. Nonexponentiality of time dependent survival probability and the fractional viscosity dependence of the rate in diffusion controlled reactions in a polymer chain nonexponentiality of time-dependent survival probability and the fractional viscosity dependence of the rate in diffusion controlled reactions in a polymer chain. *J. Chem. Phys*. 114:9170–9178.
45. Srinivas, G., A. Yethiraj, and B. Bagchi. 2001. FRET by FET and dynamics of polymer folding. *J. Phys. Chem. B*. 105:2475–2478.
46. Stultz, C. M., A. D. Levin, and E. R. Edelman. 2002. Phosphorylation-induced conformational changes in a mitogen-activated protein kinase substrate. *J. Biol. Chem*. 277:47653–47661.
47. Beierlein, F. R., O. G. Othersen, H. Lanig, S. Schneider, and T. Clark. 2006. Simulating FRET from tryptophan: is the rotamer model correct? *J. Am. Chem. Soc*. 128:5142–5152.
48. Gustiananda, M., J. R. Liggins, P. L. Cummins, and J. E. Gready. 2004. Conformation of prion protein repeat peptides probed by FRET measurements and molecular dynamics simulations. *Biophys. J*. 86: 2467–2483.
49. Jordanides, X. J., M. J. Lang, X. Song, and G. R. Fleming. 1999. Solvation dynamics in protein environments studied by photon echo spectroscopy. *J. Phys. Chem. B*. 103:7995–8005.
50. Kepka, A. G., and L. I. Grossweiner. 1973. Photodynamic inactivation of lysozyme by eosin. *Photochem. Photobiol*. 18:49–61.
51. Baugher, J. F., L. I. Grossweiner, and C. Lewis. 1974. Intramolecular energy-transfer in lysozyme-eosin complex. *J. Chem. Soc. Faraday II*. 70:1389–1398.
52. Chang, M. C., A. J. Cross, and G. R. Fleming. 1983. Internal dynamics and overall motion of lysozyme studied by fluorescence depolarization of the eosin lysozyme complex. *J. Biomol. Struct. Dyn*. 1:299–318.
53. Cross, A. J., and G. R. Fleming. 1986. Influence of inhibitor binding on the internal motions of lysozyme. *Biophys. J*. 50:507–512.
54. Adams, S. R., R. E. Campbell, L. A. Gross, B. R. Martin, G. K. Walkup, Y. Yao, J. Llopis, and R. Y. Tsien. 2002. New biarsenical ligands and tetracysteine motifs for protein labeling in vitro and in vivo: synthesis and biological applications. *J. Am. Chem. Soc*. 124:6063–6076.
55. Wang, J., R. M. Wolf, J. W. Caldwell, P. A. Kollman, and D. A. Case. 2004. Development and testing of a general AMBER force field. *J. Comput. Chem*. 25:1157–1174.
56. Cornell, W. D., P. Cieplak, C. I. Bayly, I. R. Gould, K. M. Merz, D. M. Ferguson, D. C. Spellmeyer, T. Fox, J. W. Caldwell, and P. A. Kollman. 1995. A second generation force field for the simulation of proteins, nucleic acids, and organic molecules. *J. Am. Chem. Soc*. 117:5179–5197.
57. Case, D. A., T. A. Darden, T. E. Cheatam, III, C. L. Simmerling, J. Wang, R. E. Duke, R. Luo, K. M. Merz, B. Wang, D. A. Pearlman, M. Crowley, S. Brozell, V. Tsui, H. Gohlke, J. Mongan, J. Hornak, G. Cui, P. Beroza, C. Schafmeister, J. W. Caldwell, W. S. Ross, and P. A. Kollman. 2004. AMBER 8. University of California, San Francisco, San Francisco, CA.
58. Bytheway, I., and M. W. Wong. 1998. The prediction of vibrational frequencies of inorganic molecules using density functional theory. *Chem. Phys. Lett*. 282:219–226.
59. Frisch, M. J., G. W. Trucks, H. B. Schlegel, G. E. Scuseria, M. A. Robb, J. R. Cheeseman, V. G. Zakrzewski, J. J. A. Montgomery, R. E. Stratmann, J. C. Burant, S. Dapprich, J. M. Millam, A. D. Daniels, K. N. Kudin, M. C. Strain, O. Farkas, J. Tomasi, V. Barone, M. Cossi,

R. Cammi, B. Mennucci, C. Pomelli, C. Adamo, S. Clifford, J. Ochterski, G. A. Petersson, P. Y. Ayala, Q. Cui, K. Morokuma, D. K. Malick, A. D. Rabuck, K. Raghavachari, J. B. Foresman, J. Cioslowski, J. V. Ortiz, A. G. Baboul, B. B. Stefanov, G. Liu, A. Liashenko, P. Piskorz, I. Komaromi, R. Gomperts, R. L. Martin, D. J. Fox, T. Keith, M. A. Al-Laham, C. Y. Peng, A. Nanayakkara, C. Gonzalez, M. Challacombe, P. M. W. Gill, B. Johnson, W. Chen, M. W. Wong, J. L. Andres, M. Head-Gordon, E. S. Replogle, and J. A. Pople. 1998. Gaussian 98. Gaussian, Wallingford, CT.

60. Bayly, C. I., P. Cieplak, W. D. Cornell, and P. A. Kollman. 1993. A well-behaved electrostatic potential based method using charge restraints for determining atom-centered charges: the RESP model. *J. Phys. Chem.* 97:10269–10280.
61. Cieplak, P., W. D. Cornell, C. Bayly, and P. A. Kollman. 1995. Application of the multimolecule and multiconformational RESP methodology to biopolymers: charge derivation for DNA, RNA, and proteins. *J. Comput. Chem.* 16:1357–1377.
62. Dong, J., T. J. Boggon, N. E. Chayen, J. Raftery, R.-C. Bi, and J. R. Helliwell. 1999. Bound-solvent structures for microgravity-, ground control-, gel- and microbatch-grown hen egg-white lysozyme crystals at 1.8 Å resolution. *Acta Crystallogr.* D55:745–752.
63. Machida, M., N. Ushijima, M. I. Machida, and Y. Kanaoka. 1975. N-(7-dimethylamino-4-methyl-coumarinyl)maleimide (DACM): novel fluorescent thiol reagents. *Chem. Pharm. Bull.* (*Tokyo*). 23:1385–1386.
64. Machida, M., N. Ushijima, M. I. Machida, and Y. Kanaoka. 1977. A novel fluorescent thiol reagent: Syntheses and electronic spectra of *n*-(7-dimethylamino-4-methyl-3-coumarinyl)-maleimide (DACM-3) and the related compounds. *Chem. Pharm. Bull.* (*Tokyo*). 25:1285–1288.
65. Darden, T., D. York, and L. Pedersen. 1993. Particle mesh Ewald: an *N* log*N* method for Ewald sums in large systems. *J. Chem. Phys.* 98: 10089–10092.
66. York, D. M., T. A. Darden, and L. G. Pedersen. 1993. The effect of long-range electrostatic interactions in simulations of macromolecular crystals: a comparison of the Ewald and truncated list methods. *J. Chem. Phys.* 99:8345–8348.
67. Ryckaert, J. P., G. Ciccotti, and H. J. C. Berendsen. 1977. Numerical integration of Cartesian equations of motion of a system with constraints—molecular dynamics of *n*-alkanes. *J. Comput. Phys.* 23:327–341.
68. Haas, E., E. Katchalski-Katzir, and I. Z. Steinberg. 1978. Effect of the orientation of donor and acceptor on the probability of energy transfer involving electronic transitions of mixed polarization. *Biochemistry.* 17:5064–5070.
69. Ruggiero, A. J., D. C. Todd, and G. R. Fleming. 1990. Subpicosecond fluorescence anisotropy studies of tryptophan in water. *J. Am. Chem. Soc.* 112:1003–1014.
70. Hansen, J. E., S. J. Rosenthal, and G. R. Fleming. 1992. Subpicosecond fluorescence depolarization studies of tryptophan and tryptophanyl residues of proteins. *J. Phys. Chem.* 96:3034–3040.
71. Lakowicz, J. R. 1999. Principles of Fluorescence Spectroscopy. Kluwer Academic/Plenum Publishers, Dordrecht, The Netherlands.
72. Valeur, B., and G. Weber. 1977. Resolution of the fluorescence excitation spectrum of indole into the 1la and 1lb excitation bands. *Photochem. Photobiol.* 25:441–444.
73. Cross, A. J., and G. R. Fleming. 1984. Analysis of time-resolved fluorescence anisotropy decays. *Biophys. J.* 46:45–56.
74. Horng, M. L., J. A. Gardecki, A. Papazyan, and M. Maroncelli. 1995. Subpicosecond measurements of polar solvation dynamics: Coumarin 153 revisited. *J. Phys. Chem.* 99:17311–17337.
75. Lewis, J. E., and M. Maroncelli. 1998. On the (uninteresting) dependence of the absorption and emission transition moments of coumarin 153 on solvent. *Chem. Phys. Lett.* 282:197–203.
76. Fleming, G. R., A. W. E. Knight, J. M. Morris, R. J. S. Morrison, and G. W. Robinson. 1977. Picosecond fluorescence studies of xanthene dyes. *J. Am. Chem. Soc.* 99:4306–4311.
77. Walker, R. C., I. P. Mercer, I. R. Gould, and D. R. Klug. 2006. A comparison of basis set effects and the performance of ab initio and DFT methods for probing equilibrium fluctuations. *J. Comput. Chem.* 28:478–490.
78. Zwier, M. C., J. M. Shorb, and B. P. Krueger. 2007. Hybrid molecular dynamics-quantum mechanics simulations of solute spectral properties in the condensed phase: evaluation of simulation parameters. *J. Comput. Chem.* In press.
79. Reference deleted in proof.
80. Chang, J. C. 1977. Monopole effects on electronic excitation interactions between large molecules. I. Application to energy transfer in chlorophylls. *J. Chem. Phys.* 67:3901–3909.
81. Krueger, B. P., G. D. Scholes, and G. R. Fleming. 1998. Calculation of couplings and energy-transfer pathways between the pigments of lh2 by the ab initio transition density cube method. *J. Phys. Chem. B.* 102: 5378–5386, 9603.
82. Scholes, G. D., I. R. Gould, R. J. Cogdell, and G. R. Fleming. 1999. Ab initio molecular orbital calculations of electronic coupling in the lh2 bacterial light-harvesting complex of *Rps. acidophila*. *J. Phys. Chem. B.* 103:2543–2553.
83. Wong, K. F., B. Bagchi, and P. J. Rossky. 2004. Distance and orientation dependence of excitation transfer rates in conjugated systems: beyond the Förster theory. *J. Phys. Chem. A.* 108:5752–5763.
84. Humphrey, W., A. Dalke, and K. Schulten. 1996. VMD—visual molecular dynamics. *J. Mol. Graph.* 14:33–38.